# Energy transfer dynamics in an RC–LH1–PufX tubular photosynthetic membrane

**J Hsin**[1,4], **J Strümpfer**[2,4], **M Şener**[1], **P Qian**[3], **C N Hunter**[3] **and K Schulten**[1,2,5]

[1] Department of Physics and Beckman Institute, University of Illinois at Urbana-Champaign, Urbana, USA
[2] Center for Biophysics and Computational Biology and Beckman Institute, University of Illinois at Urbana-Champaign, Urbana, USA
[3] Department of Molecular Biology and Biotechnology, University of Sheffield, Sheffield S10 2TN, UK
E-mail: kschulte@ks.uiuc.edu

**Abstract.** Light absorption and the subsequent transfer of excitation energy are the first two steps in the photosynthetic process, carried out by protein-bound pigments, mainly bacteriochlorophylls (BChls), in photosynthetic bacteria. BChls are anchored in light-harvesting (LH) complexes, such as light-harvesting complex I (LH1), which directly associates with the reaction center (RC), forming the RC–LH1 core complex. In *Rhodobacter sphaeroides*, RC–LH1 core complexes contain an additional protein, PufX, and assemble into dimeric RC–LH1–PufX core complexes. In the absence of LH complex II (LH2), the former complexes can aggregate into a helically ordered tubular photosynthetic membrane. We have examined the excitation transfer dynamics in a single RC–LH1–PufX core complex dimer using the hierarchical equations of motion for dissipative quantum dynamics that accurately, yet in a computationally costly manner, treat the coupling between BChls and their protein environment. A widely employed description, the generalized Förster (GF) theory, was also used to calculate the transfer rates of the same excitonic system in order to verify the accuracy of this computationally cheap method. Additionally, in light of the structural uncertainties in the *Rba. sphaeroides* RC–LH1–PufX core complex,

---

geometrical alterations were introduced into the BChl organization. It is shown that the energy transfer dynamics are not affected by the considered changes in the BChl organization and that the GF theory provides accurate transfer rates. An all-atom model for a tubular photosynthetic membrane is then constructed on the basis of electron microscopy data, and the overall energy transfer properties of this membrane are computed.

## Contents

## 1. Introduction

Photosynthesis is initiated when protein-bound pigments absorb light energy [1]–[3]. In photosynthetic purple bacteria, these pigments are anchored within protein complexes, typical examples being the light-harvesting complexes I and II (LH1 and LH2) [3, 4]. The LH1 complex surrounds the reaction center (RC), forming the RC–LH1 core complex. A light-excited pigment rapidly passes its excitation energy onto nearby pigments, with the energy arriving within tens of picoseconds at the RC to be utilized then for charge separation, the starting point for later steps of photosynthesis. A light-harvesting (LH) complex consists of a few tens of bacteriochlorophylls (BChls) as well as carotenoids, which have been described by various theoretical models [3]–[8]. LH complexes further aggregate tightly in the photosynthetic membrane, forming distinct membrane vesicles and producing arrays of thousands of BChls and carotenoids [9]. Here we focus on the BChl subsystem. The role of the carotenoids feeding excitation energy into the BChl system has been studied in [6, 7, 10].

A theoretical description of the energy transfer dynamics within a BChl array requires knowledge of the geometrical arrangement of BChls. Such knowledge relies on a high-resolution structure of the LH complexes in which the BChls are bound and on information regarding the vesicle-scale packing arrangement of hundreds of LH complexes in the photosynthetic membrane. The natural heterogeneity of LH complexes brings about disorder in
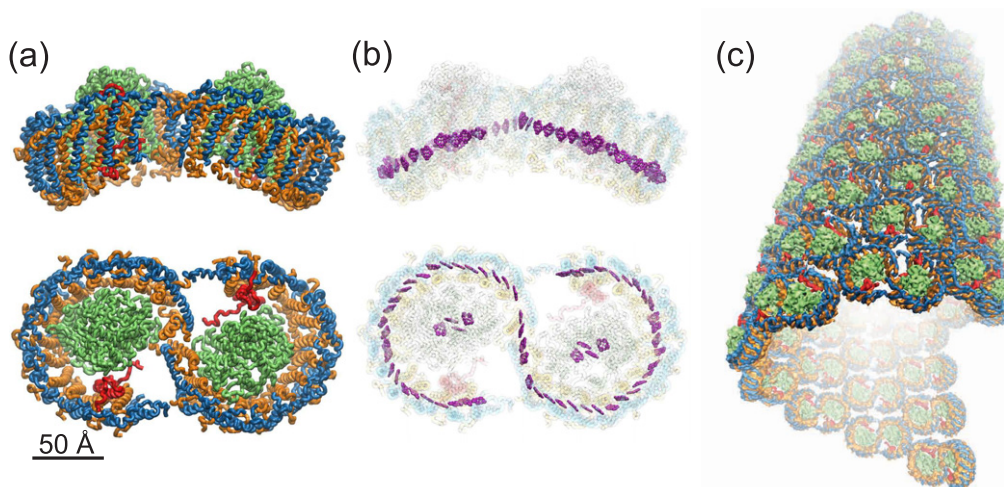
**Figure 1.** (a) Model of the *Rba. sphaeroides* RC–LH1–PufX core complex constructed in previous studies [18]–[20]. LH1$\alpha$ is shown in orange; LH1$\beta$ in blue, RC in green and PufX in red. (b) BChl array (purple). Top: side view along the membrane plane; bottom: top view. (c) A perspective view of a segment of the tubular photosynthetic membrane composed of solely RC–LH1–PufX core complexes. Molecular images in this and other figures were prepared with VMD [21].

the packing arrangement, presenting an ambiguity in the locations of complexes, as illustrated in atomic force microscopy (AFM) imaging studies [11, 12]. This disorder is avoided when only a single type of LH complex is present. For this reason, the current study focuses on the tubular membrane isolated from the LH2-deficient mutant of *Rhodobacter* (*Rba.*) *sphaeroides*, which consists of orderly and helically arranged dimeric core complexes [13]–[17] (see figure 1).

Due to the lack of a high-resolution structure for the *Rba. sphaeroides* core complex, shown in figure 1, local structural uncertainties remain. Two disputed structural features of the *Rba. sphaeroides* core complex concern the location of PufX proteins that are part of the complex, and the exact stoichiometry of LH1 subunits.

PufX is a single transmembrane polypeptide found within the *Rba. sphaeroides* core complex [4, 22]. Hence, the *Rba. sphaeroides* core complex is also referred to as the RC–LH1–PufX core complex. While an 8.5 Å-resolution two-dimensional (2D) cryo-electron microscopy (cryo-EM) projection map, currently the highest resolution structural information of the complex, places PufX near the gap of the LH1 openings [16, 23] (figure 1(a)), other studies suggest that PufX is located at the dimerizing junction of the complex [24]–[28] and, consequently, interrupting the S-shaped BChl array shown in figure 1(b). Notably, while PufX is not directly involved in the LH process, deletion of PufX leads to monomeric, ring-like, RC–LH1 complexes [22, 29], suggesting that it plays an active role in determining the oligomerization state of the *Rba. sphaeroides* core complex.

Another unresolved structural feature of the *Rba. sphaeroides* core complex is the number of LH1 subunits and BChls in each RC–LH1 monomer. The 2D cryo-EM projection map identified 14 LH1 subunits per RC, the ratio supported by a quantitative measurement of the purified complex in the same study [23]. Another study proposed a $13 \pm 1$ LH1 subunit-to-RC

ratio [30]. AFM imaging data on the core complex of *Rba. blasticus*, closely related to *Rba. sphaeroides*, was interpreted to show a 13:1 LH1 subunit-to-RC ratio [25]. As each LH1 subunit contains two BChls, the unresolved stoichiometry of LH1 implies uncertainty of the number of BChls in a core complex. This uncertainty should be taken into account when considering excitation transfer dynamics in the core complex.

A BChl originally in the ground state is excited to a higher energy state upon absorption of light energy. The excited state of BChl is denoted as the $Q_y$ state [3, 4]. This excitation is quickly shared among several BChls, forming an exciton in LH1, which is then transferred to an RC or to a nearby LH1. Exciton formation and excitation transfer depend sensitively on BChl–protein environmental coupling. Characterization of the coupling between BChls and protein has been achieved through different approaches. When the coupling between BChls is weak in comparison to the BChl–protein coupling, the excitation tends to localize and transfer incoherently between BChls, a limit that can be described by Förster theory [31]. Alternatively, when the coupling between BChls is large in comparison to the BChl–protein coupling, the protein environment can be treated using perturbative generalized master equation methods, such as the Redfield theory [32, 33]. In the case of LH1, BChl–BChl coupling is of similar strength to BChl–protein coupling, disallowing *prima facie* use of the Förster theory and requiring higher order methods than the Redfield theory [34].

In the case of the *Rba. sphaeroides* RC–LH1–PufX core complex, excitation transfer dynamics are further complicated due to the relatively strong coupling between BChls of LH1 and those of the RC, as well as due to the dimeric nature of the core complex (figure 1(b)). To calculate exciton transfer rates using the generalized Förster (GF) theory [31], donor and acceptor groups of BChls have to be defined. In systems where the BChls are distinctively separated into strongly coupled clusters, donor–acceptor partitioning is straightforward. In LH1, however, some of the BChls are strongly coupled within each monomer, and some are strongly coupled between the two monomers. Hence, the question arises whether the core complex dimer is best treated as two clusters, one consisting of the LH1 BChls and the other consisting of the RC BChls, or alternatively as four clusters, by further dividing the BChls according to which side of the dimer they reside in.

A complete description of the excitation dynamics is furnished by the hierarchical equations of motion (HEOM) for the time evolution of the density matrix. These equations were formulated by Tanimura and Kubo [35, 36]. The HEOM can be employed to investigate the excitation transfer properties within a single *Rba. sphaeroides* core complex since the equations describe the excitation dynamics, taking into account the non-Markovian nature of the evolution due to strong BChl–protein coupling, as well as the non-negligible inter-BChl coherences due to strong BChl–BChl coupling [37]. Furthermore, unlike the generalized Förster (GF) theory, the HEOM do not require the artificial partitioning of the BChls into donor/acceptor arrays. However, the extreme computational expense of the method is a limiting factor for all but the simplest systems [12, 37]. In the case of the present study, the respective calculations required 32 processors running for 32 days of wall clock time and using 100 GB of shared memory.

On the vesicle scale, coupling between the BChls in different core complexes is much weaker than the BChl–protein coupling within each complex. The excitation transfer between different core complexes can then be described in the framework of the GF theory [12]. From calculated intra- and inter-complex transfer rates, a Markovian master equation arises that describes the exciton migration across the vesicle, and from this the expected excitation lifetimes and LH efficiencies can be computed [9].

The present investigation starts with the construction of an all-atom model for the *Rba. sphaeroides* tubular photosynthetic membrane consisting of only the core complex dimers (figure 1(c)). Characterization of the energy transfer properties begins at the single-complex level, using both the GF formulation and the HEOM, employing also two partitioning schemes where donor and acceptor groups of BChls are defined differently. A comparison of the two descriptions is aimed at determining whether the GF theory provides accurate results and what partitioning scheme is most appropriate. Next, variations in BChl organization within the core complex are introduced to cover all prior suggestions regarding the structural characteristics of the complex. Lastly, the LH efficiency and excitation lifetime of the modeled tubular membrane of core complexes are calculated.

## 2. Methods

### 2.1. Construction of the RC–LH1–PufX core complex model

The *Rba. sphaeroides* RC–LH1–PufX core complex model was constructed in a series of homology modeling and computational studies based on available structural data [18]–[20]. The construction is summarized here. The model was built using solution structures of LH1$\beta$ and PufX [38, 39], the structure of the RC [40, 41] and homology modeling of LH1$\alpha$ based on the solution structure of LH1$\alpha$ of *Rhodospirillum rubrum* [42]. The proteins were then assembled in an arrangement proposed by an 8.5 Å-resolution cryo-EM projection map [23]. Since this projection map did not provide structural information about the bending of the complex normal to the membrane plane, the RC–LH1–PufX dimer was modeled initially as a 'flat' transmembrane complex [18]. Interestingly, subsequent molecular dynamics simulations revealed a strong tendency of the core complex to bend [18].

3D structural data on the *Rba. sphaeroides* core complex became available through a single-particle EM reconstruction study at 25 Å resolution [17], which showed that the dimeric complex is highly bent, i.e. 'V-shaped' when viewed along the membrane plane. To induce a similarly bent geometry in the model developed in [18], the molecular dynamics flexible fitting method [43]–[45] was employed. This approach provided an atomic structure of the core complex dimer that was stable over tens of nanoseconds simulation time and exhibited the correct bent geometry and membrane-bending properties [20] (figure 1(a)). The atomic model also contains the BChls, as shown in figure 1(b).

### 2.2. Variations in the local geometry in the BChl array

Due to a lack of a high-resolution structure for the full core complex, ambiguities remain for some features in the molecular arrangement within the complex. In particular, alternative placements for PufX have been proposed. One placement positions one PufX near each opening of the LH1 ring [16, 19, 20, 23, 29, 46], in which case the BChls in LH1 form a continuous, S-shaped array (figures 1(b), 2(a) and 2(b)). The other placement puts two PufX at the dimerization junction of the core complex [24]–[28], consequently interrupting the S-shaped BChl array with a gap at the center of the dimer (figure 2(c)).

Ambiguities also remain regarding the precise LH1 subunit to RC ratio. The 2D cryo-EM projection map suggests 14 LH1 subunits per RC and, in the same study, a quantitative analysis of the purified complex yielded a $28 \pm 2.2$ BChl to RC ratio [23], i.e. $56 \pm 4.4$ LH1 BChls per
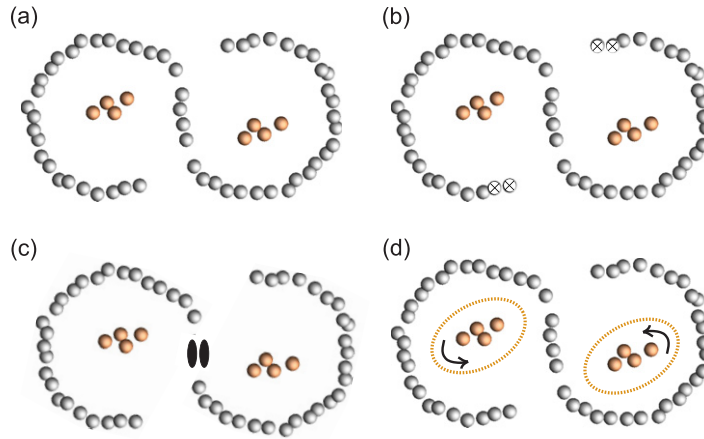
**Figure 2.** BChl arrays within the core complex investigated. (a) BChl array of 56 contiguous BChls suggested in [19, 23]. LH1 BChls are shown as filled gray circles and RC BChls are shown as filled orange circles. (b) BChl array as in (a), but with only 52 contiguous BChls; the deleted BChls are shown as empty circles with crosses. (c) BChl array with a gap at the dimerizing junction of the core complex due to the placement of PufX; the two PufX proteins are shown as black ovals. (d) Rotation of the RC BChls within their respective LH1 rings.

core complex. Other studies suggested, however, a ratio of $13 \pm 1$ LH1 subunits per RC [25, 30] or equivalently $52 \pm 4$ LH1 BChls per complex.

To determine the effect of variation in the BChl organization on the energy transfer dynamics in the core complex, four different BChl arrays were created, as shown in figure 2. Figure 2(a) displays the BChl array resulting from previous modeling [18]–[20], involving a continuous array of 56 LH1 BChls. Figure 2(b) displays an array where there are only 52 LH1 BChls. Figure 2(c) displays a BChl array that exhibits a gap at the center due to the placement of PufX there. Rotation of the RCs in the core complex, discussed below, is shown in figure 2(d).

### 2.3. Theoretical descriptions of excitation transfer

A description in terms of an effective Hamiltonian, widely applied to LH systems [3, 5, 6, 9, 19, 33], [47]–[58], is employed here to characterize the excitonic system of the core complex. The effective Hamiltonian for a single complex,

$$H = \sum_j E_j |j\rangle\langle j| + \sum_{j,k} V_{jk} |j\rangle\langle k|, \tag{1}$$

is stated in the basis of $Q_y$ excited states of BChl at site $j$. $E_j$ denotes the energy of the $Q_y$ state of BChl $j$ and $V_{jk}$ denotes the interaction energy between BChls $j$ and $k$. The Hamiltonian is diagonalized to obtain the eigenstates $|\varepsilon_\alpha\rangle$ and eigenenergies $\varepsilon_\alpha$ of the array. In the diagonal form it is

$$H = \sum_\alpha \varepsilon_\alpha |\varepsilon_\alpha\rangle\langle\varepsilon_\alpha|. \tag{2}$$

The Förster theory accurately calculates the transfer of excitation energy between BChls that interact only weakly. In this regime, the excitation is localized on a single BChl and, after light

excitation, no quantum coherence arises between the BChls. The Förster transfer rate from BChl 1 to BChl 2 is derived from Fermi's golden rule [31],

$$k_{12}^{\mathrm{F}} = \frac{2\pi}{\hbar} V_{12}^2 J_{12}, \tag{3}$$

where $V_{12}$ is the electronic interaction energy between BChls 1 and 2, and $J_{12}$ is the spectral overlap between the fluorescence lineshape of BChl 1 and the absorption lineshape of BChl 2.

The GF theory extends the Förster theory to calculate the excitation transfer rate between donor and acceptor BChl arrays as opposed to that between single BChl molecules. The generalization is introduced since the intra-array electronic coupling is much stronger than the inter-array electronic coupling [59]–[61]. The GF theory assumes that, after initial excitation, as well as after any donor array → acceptor array excitation transfer, the donor array or, respectively, the acceptor array quickly (i.e. on a timescale much shorter than the exciton transfer time) thermalizes to a Boltzmann distribution of exciton states. In analogy to Förster transfer between weakly coupled BChls, the excitation is 'localized' on the donor array and transfers incoherently to the acceptor array. Within the donor array, however, the excitation is coherently delocalized and forms exciton states. The exciton states of the donor array thus transfer excitation incoherently to the exciton states of the acceptor array. After excitation transfer, the same happens in the acceptor array, which becomes the donor array for the next excitation transfer event.

The total excitation transfer rate between donor and acceptor arrays of BChls, according to the GF theory, is [3, 47, 54, 59], [61]–[64]

$$k_{\mathrm{D}\to\mathrm{A}} = \frac{2\pi}{\hbar} \sum_{\alpha \in \mathrm{D}} \sum_{\beta \in \mathrm{A}} \frac{\exp(-\varepsilon_\alpha^{\mathrm{D}}/k_{\mathrm{B}}T)}{Z} \left| \langle \varepsilon_\alpha^{\mathrm{A}} | H_{\mathrm{DA}} | \varepsilon_\beta^{D} \rangle \right|^2 J_{\mathrm{DA}}. \tag{4}$$

Here, $Z = \sum_\alpha \exp(-\varepsilon_\alpha^{\mathrm{D}}/k_{\mathrm{B}}T)$ is the partition function and $J_{\mathrm{DA}}$ is the spectral overlap of donor and acceptor BChl lineshapes. $\alpha$ and $\beta$ denote exciton states of donor and acceptor BChl arrays, respectively, defined in equation (2).

To calculate the transfer rate using equation (4), donor and acceptor arrays of BChls have to be defined, i.e. BChls have to be clustered according to interaction strength. It is not always straightforward, however, to cluster BChls with a broad distribution of coupling strengths into donor and acceptor arrays. Below we will compare transfer rates resulting from different partitioning schemes.

The density matrix $\rho(t) = \sum_{i,j} \rho_{ij}(t)|i\rangle \langle j|$ contains the information concerning the quantum state of the excited BChl system. $\rho_{ii}(t)$ describes the probability of finding BChl $i$ in the $Q_y$ excited state, which we call the population of BChl $i$ hereafter. $\rho_{ij}(t), i \neq j$, describes the coherence between excited BChls $i$ and $j$. An excited BChl system in contact with a thermal bath requires a description involving the time evolution of a bath-averaged density matrix. Much effort has been made to theoretically model such time evolution using so-called dissipative quantum mechanics [65].

The Redfield theory treats the system–bath coupling perturbatively and applies when the system–bath coupling is small compared to the interactions of the excited states [32, 33]. Modified Redfield theory overcomes this limitation by ignoring the time evolution of the coherence terms $\rho_{ij}(t), i \neq j$ [33, 37, 66]. However, nearest-neighbor BChls in LH1 are strongly interacting [19], such that one cannot decouple the corresponding coherence terms from the populations. Furthermore, interaction between the bath and BChls is of the same order of magnitude as nearest-neighbor BChl interactions [67]. As a result, the bath cannot be treated

as a perturbation to the system, and neither the Redfield theory nor modified Redfield theory is applicable [34].

Instead, we employ the HEOM of Tanimura and Kubo [35, 36, 68]. The time evolution of the density matrix is computed using the HEOM, taking into account non-Markovian bath effects by employing auxiliary density matrices. The description of the thermal bath enters through the bath spectral density $J_i(\omega)$, which describes the coupling strength of the normal mode of frequency $\omega$ in the local protein environment to the $Q_y$ excited state of BChl $i$ [69]. For $J_i(\omega)$, we assume the often employed Debye form,

$$J_i(\omega) = 2\lambda_i \gamma_i \frac{\omega}{\gamma_i^2 + \omega^2}. \tag{5}$$

Due to the similarity of the environments of each BChl, each BChl experiences the same spectral density $J_i(\omega)$. For each BChl $i$, the reorganization energy is assumed to be $\lambda_i = 250\,\text{cm}^{-1}$ and the bath response time to be $1/\gamma_i = 100\,\text{fs}$. These values have been chosen to match experimental results [67, 70]. It is important to note that, in the present description, the environmental fluctuations of each BChl are assumed to be uncorrelated with those of its neighbors. This is possibly a shortcoming of the suggested description.

To describe the evolution of $\rho(t)$ after initial light absorption, the Hamiltonian in equation (1) is modified to account for dissipation of excitation into the bath and use of excitation energy by the special pair BChls of the RC to generate a charge-separated state. For this purpose, two non-Hermitian terms are added conventionally [71, 72], resulting in the new Hamiltonian

$$H_\text{T} = H + i\hbar \sum_{i=1}^{N} k_\text{diss}|i\rangle\langle i| + i\hbar \sum_{i \in SP} k_\text{cs}|i\rangle\langle i|. \tag{6}$$

The dissipation rate constant is $k_\text{diss} = 1\,\text{ns}^{-1}$ and the charge separation rate constant is $k_\text{cs} = \frac{1}{3}\,\text{ps}^{-1}$ (9). Here, $i = 1, 2, \ldots, N$ labels both LH1 and RC BChls; $i \in SP$ labels the two special pair BChls in the RC [47]. The derivation of the HEOM that describes the time evolution of $\rho(t)$ is outlined in [12] for the case of the Debye spectral density defined in equation (5). In the present study, we employ the time-non-local truncation of the equation hierarchy [73] along with the Ishizaki–Tanimura temperature correction terms [36].

To explore excitation migration in the BChl system, two partition schemes are investigated, as shown in figure 3. Partition scheme I (figure 3(a)) describes the core complex as two BChl arrays, one comprising all the BChls in LH1 and the other comprising all the BChls in both RCs. Partition scheme II (figure 3(b)) further separates each half of the dimeric complex, resulting in four BChl arrays: the left half of LH1, the left RC, the right half of LH1 and the right RC. Excitation transfer events can occur between all BChl arrays.

The populations of each BChl array can be calculated from $\rho(t)$ by adding up the BChl populations, i.e. $\rho_{ii}(t)$, with indices $i$ corresponding to BChls $i$ in the respective array. The time evolution of the array populations can be fitted to a kinetic model that corresponds to incoherent inter-array population transfer.

The kinetic equations describing partition scheme I are

$$\dot{P}_\text{LH1} = -\left(k_{\text{LH1}\rightarrow\text{RC}} + k_\text{diss}\right) P_\text{LH1} + k_{\text{RC}\rightarrow\text{LH1}} P_\text{RC}, \tag{7a}$$

$$\dot{P}_\text{RC} = -\left(k_{\text{RC}\rightarrow\text{LH1}} + k_\text{cs}\right) P_\text{RC} + k_{\text{LH1}\rightarrow\text{RC}} P_\text{LH1}. \tag{7b}$$
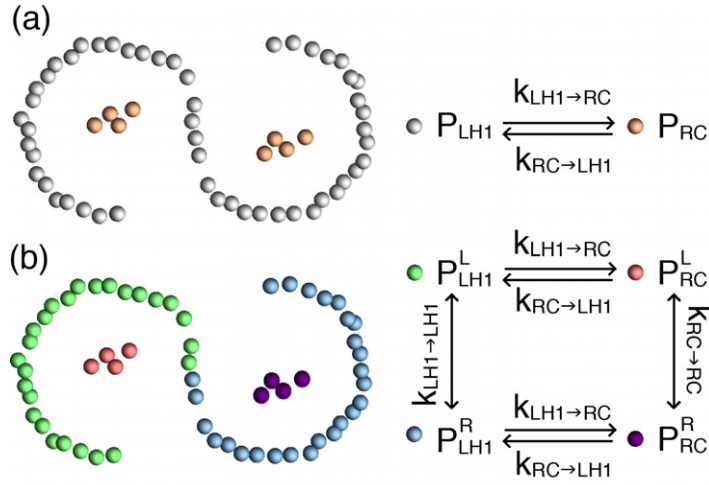
**Figure 3.** Schemes employed to partition the BChls of the core complex. (a) Partition scheme I consists of two BChl arrays; $P_{LH1}$ is shown in gray and $P_{RC}$ in orange. (b) Partition scheme II contains four BChl arrays: $P_{LH1}^{L}$ in green, $P_{LH1}^{R}$ in blue, $P_{RC}^{L}$ in red and $P_{RC}^{R}$ in purple.

Here, the LH1 population, $P_{LH1}$, is the total probability of finding LH1 BChls in the $Q_y$ excited state, and the RC population, $P_{RC}$, is the total probability of finding the RC BChls in the $Q_y$ excited state. The kinetic equations for partition scheme II are

$$\dot{P}_{LH1}^{L} = -\left(k_{LH1\to RC} + k_{LH1\to LH1} + k_{diss}\right) P_{LH1}^{L} + k_{LH1\to LH1} P_{LH1}^{R} + k_{RC\to LH1} P_{RC}^{L}, \tag{8a}$$

$$\dot{P}_{LH1}^{R} = -\left(k_{LH1\to RC} + k_{LH1\to LH1} + k_{diss}\right) P_{LH1}^{R} + k_{LH1\to LH1} P_{LH1}^{L} + k_{RC\to LH1} P_{RC}^{R}, \tag{8b}$$

$$\dot{P}_{RC}^{R} = -\left(k_{RC\to LH1} + k_{RC\to RC} + k_{cs}\right) P_{RC}^{R} + k_{LH1\to RC} P_{LH1}^{R} + k_{RC\to RC} P_{RC}^{L}, \tag{8c}$$

$$\dot{P}_{RC}^{L} = -\left(k_{RC\to LH1} + k_{RC\to RC} + k_{cs}\right) P_{RC}^{L} + k_{LH1\to RC} P_{LH1}^{R} + k_{RC\to RC} P_{RC}^{R}. \tag{8d}$$

The populations $P_{LH1}$ and $P_{RC}$ have been split according to which half of the dimer they reside in (left side or right side can be assigned arbitrarily due to the symmetry of the core complex). The transfer rate constants $k_{RC\to RC}$, $k_{LH1\to RC}$, $k_{RC\to LH1}$ and $k_{LH1\to LH1}$ in equations (7) and (8) can be determined directly using the GF theory (equation (4)) or by fitting to the time evolution of the BChl array populations provided by $\rho(t)$. These rate constants for excitation transfer are defined in figure 3.

Both equations (7) and (8) can be expressed in the form $\dot{\mathbf{P}} = \mathbf{MP}$, with M being the transition matrix and $\mathbf{P}$ the vector of populations (i.e. $\mathbf{P} = (P_{LH1}, P_{RC})^{T}$ for scheme I and $\mathbf{P} = (P_{LH1}^{L}, P_{LH1}^{R}, P_{RC}^{L}, P_{RC}^{R})^{T}$ for scheme II). This allows one to determine the LH efficiency $\eta$, i.e. the probability that an excitation reaches a charge separated state, and the excitation lifetime $\tau$ (derivations of $\eta$ and $\tau$ can be found in [9]),

$$\eta = -2k_{cs} \sum_{\ell \in RC} \left(M^{-1}\mathbf{P}(0)\right)_{\ell}, \tag{9}$$

$$\tau = \frac{-2k_{cs}}{\eta} \sum_{\ell \in RC} \left(M^{-2}\mathbf{P}(0)\right)_{\ell}, \tag{10}$$
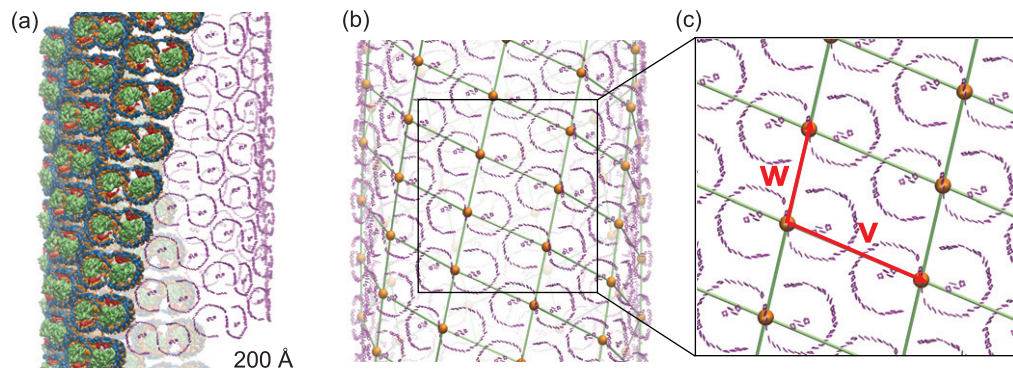
**Figure 4.** The tubular membrane model and its periodic architecture. (a) The all-atom model of the helically arranged core complex dimers forming a tubular photosynthetic membrane. Full complexes are shown on the left half of the tube, with only the BChl arrays shown on the right half to illustrate the long-range organization of multiple BChl arrays. (b) Network defined by connecting the symmetry axes of core complexes constituting the membrane. The projection of this network onto a plane results in the periodic tiling shown in (c), the symmetry of which corresponds to the wallpaper group **p2** [75]. The vectors **v** and **w** span the basic cell of the tiling and obey equation (11).

where $\ell$ labels the BChl array. For scheme I, the set RC consists of a single entry that includes all BChls in both RCs and M is a $2 \times 2$ matrix. For scheme II, the set RC consists of two entries, one for the BChls in each RC and M is a $4 \times 4$ matrix.

## 3. Results

Below we describe the construction of an atomic model of the tubular photosynthetic membrane consisting of the RC–LH1–PufX core complex. Due to uncertainties in the structure of the *Rba. sphaeroides* core complex, the LH kinetics are calculated for different BChl arrangements in the core complex dimers (see figure 2). Both the GF theory and the HEOM are applied and the results compared. We then present calculations addressing inter-complex excitation transfers. Finally, the excitation dynamics in tubular membranes filled with helically arranged core complexes is characterized.

### 3.1. Construction of the tubular photosynthetic membrane

The *Rba. sphaeroides* core complex model developed in [18]–[20] (see section 2) was used for the construction of the tubular photosynthetic membrane as experimentally characterized through EM [13]–[17], [74] and shown in figure 1(c). For this purpose, the atomic coordinates of the modeled complex were replicated and arranged into a cylindrical array using the molecular visualization package VMD [21], with the placements of the complexes determined from EM images of the native *Rba. sphaeroides* tubular photosynthetic membrane [17]. The resulting model of the tubular membrane is shown in figure 4(a). The periodicity of the ordered arrangement of the complexes is shown in figures 4(b) and 4(c).

**Table 1.** Transfer rate constants, LH efficiencies and excitation lifetimes of a single core complex modeled with PufX placed near the gaps of LH1 calculated using the kinetic model with HEOM-fitted and with GF rate constants.

| Theoretical framework | $\rho(t)$ | | GF | |
|---|---|---|---|---|
| Partition scheme [a] | I | II | I | II |
| $k_{\text{LH1}\rightarrow\text{RC}}$ (ps$^{-1}$) | 1/63.0 | 1/60.6 | 1/58.26 | 1/59.5 |
| $k_{\text{RC}\rightarrow\text{LH1}}$ (ps$^{-1}$) | 1/16.0 | 1/10.1 | 1/8.5 | 1/8.6 |
| $k_{\text{LH1}\rightarrow\text{LH1}}$ (ps$^{-1}$)[b] | | 1/2.9 | | 1/3.5 |
| $k_{\text{RC}\rightarrow\text{RC}}$ (ps$^{-1}$)[b] | | 1/13.96 | | 1/10\,000 |
| LH efficiency $\eta$ (%) | 93.4 | 93.4 | 92.7 | 92.4 |
| Excitation lifetime $\tau$ (ps) | 66.5 | 66.1 | 74.5 | 76.6 |

[a] cf figure 3.
[b] Applicable to partition scheme II only.

Tubular structures constructed by the periodic assemblies of identical units have been reported for numerous biological systems, the best known case being viral capsids [76]. The mathematical theory of tiling [75] provides a concise description for an orderly, tubular structure. It has been employed, for example, to classify viral capsid morphologies [77, 78].

According to the theory of tiling, the periodicity in the arrangement of the core complex dimers in the tubular membrane model is preserved, as illustrated in figure 4. The arrangement of the core complexes is characterized by parameters **v**, **w** and $R$. **v** and **w** are 2D vectors defining the basic cell of the tiling and are estimated from [17]. $R$ is the radius of the tube. The cylindrical geometry imposes the condition

$$m\mathbf{v} + n\mathbf{w} = (2\pi R, 0), \tag{11}$$

where $n$ and $m$ are positive integers. The geometry depicted in figure 4 corresponds to $m = 10$ and $n = 6$, with an outer radius $R_{\text{o}}$ of 340 Å.

### 3.2. Excitation dynamics in a single core complex

Prior to computing the excitation dynamics in the full tubular photosynthetic membrane depicted in figure 4, structural uncertainties within the *Rba. sphaeroides* core complex are addressed by considering different BChl arrangements, as shown in figure 2. For the theoretical description, we employ the GF formulation and the HEOM.

The HEOM describe the excitation dynamics in the core complex without reference to a partitioning scheme, as shown in figure 3. Nevertheless, the kinetic model corresponding to one or the other partitioning scheme, as defined in equations (7) and (8), can be fitted to the results of the HEOM calculations. Such a fit yields transfer rate constants that are listed in tables 1 and 2. This treatment, calculation of $\rho(t)$ and fit of exciton population dynamics to kinetic schemes corresponding to the two partitioning schemes defined in figure 3, has been applied to both placements of PufX, as shown in figures 2(b) and (c). In the case of a GF description, transfer rate constants can be calculated directly and plugged into the kinetic models right away.

The results of the respective computations are presented in the supplementary data (available from stacks.iop.org/NJP/12/085005/mmedia) accompanying this paper. In summary,

**Table 2.** Transfer rate constants, LH efficiencies and excitation lifetimes of a single core complex modeled with PufX placed at the center of the complex described using the kinetic model with HEOM-fitted and with GF rate constants.

| Theoretical framework | $\rho(t)$ | | GF | |
|---|---|---|---|---|
| Partition scheme [a] | I | II | I | II |
| $k_{LH1 \to RC}$ $(0^{-1})$ | 1/58.6 | 1/58.2 | 1/59.1 | 1/59.8 |
| $k_{RC \to LH1}$ $(ps^{-1})$ | 1/13.5 | 1/13.0 | 1/8.8 | 1/8.6 |
| $k_{LH1 \to LH1}$ $(ps^{-1})$[b] | | 1/35.3 | | 1/82.5 |
| $k_{RC \to RC}$ $(ps^{-1})$[b] | | 1/30.4 | | 1/9178 |
| LH efficiency $\eta$ (%) | 93.8 | 93.7 | 92.3 | 92.4 |
| Excitation lifetime $\tau$ (ps) | 62.6 | 62.5 | 75.8 | 75.6 |

[a] cf figure 3.
[b] Applicable to partition scheme II only.

we find that the kinetic model describes very well the population dynamics calculated from the HEOM for either placement of PufX and for either partitioning scheme (figures S1–S4). This implies that there is negligible coherent transfer of excitation between the BChl clusters defined in figure 3.

The time evolution of the excited state populations calculated with the kinetic model using GF transfer rate constants also closely matches the time evolution computed by the HEOM. An exception is, however, the population dynamics seen in the case of the center placement of PufX (figure 2(c)) employing partition scheme II (figure 3(b)). The population dynamics are shown in figures S3 and S4. The discrepancy in this case is due to the intra-LH1 transfer rate constant, $k_{LH1 \to LH1}$, which in the GF theory is small in comparison to that obtained from a kinetic model fit to the HEOM results (see table 2). The excitation transfer rate constants calculated from fitting the kinetic model to the HEOM and from the GF theory are presented in the following section.

### 3.3. Excitation transfer in a single core complex

While the methods employed here permit a full description of the excitation dynamics, the results of interest are the excitation transfer rates between BChl clusters. Tables 1 and 2 summarize the transfer rate constants obtained by fitting the kinetic model (equations (7) and (8)) to $\rho(t)$ calculated from the HEOM and from the GF theory for either the partitioning scheme or placement of PufX. It is seen that, for either scheme, there is little difference between the two PufX placements (figures 2(b) and (c)) in regard to the LH1 → RC and RC → LH1 transfer rate constants, $k_{LH1 \to RC}$ and $k_{RC \to LH1}$. The gap in the array of LH1 BChls (figure 2(c)) is seen to affect only the intra-LH1 transfer rate constant, $k_{LH1 \to LH1}$.

Calculations of LH efficiency, $\eta$, and average excitation lifetime, $\tau$, for a single core complex were performed using equations (9) and (10) (see section 2). For either partitioning scheme and placement of PufX, only a small difference arises in the LH efficiency (1% difference). A more noticeable difference of 10 ps in the average excitation lifetime is seen when comparing the results of the HEOM and the GF theory, the difference arising from the

relatively faster RC → LH1 transfer calculated through the GF theory. The GF theory also tends to underestimate the transfer rate constant between the halves of the dimer ($k_{LH1 \to LH1}$) since the BChls at the center of the complex have a high coupling strength ($23\,cm^{-1}$ for the center placement of PufX), in which case the GF theory is not accurate.

In the present model, there are 52 LH1 BChls in each core complex, i.e. the LH1 subunit to RC ratio is 13, as suggested in [25, 30] (figures 2(b) and 2(c)). However, an LH1 to RC ratio of 14 was resolved in the 2D cryo-EM projection map [23], currently the highest resolution structural information of the complex. This ratio, corresponding to 56 BChls per complex (figure 2(a)), needs to be considered here. Using the GF theory, the excitation lifetime for the BChl array depicted in figure 2(a) is computed to be 75.6 ps, comparable to the lifetime of other BChl arrangements in tables 1 and 2. The excitation transfer rate seems to be insensitive to the slight change in BChl stoichiometry.

The transfer rates computed here agree well with prior experimental results. The time for forward transfer (LH1 → RC) in the core complex was measured to be within the range of 30–50 ps [19], [79]–[83]. The backtransfer time (RC → LH1) was reported to be ∼8 ps [19, 79], which is consistent with the values of $k_{LH1 \to RC}$ and $k_{RC \to LH1}$ listed in tables 1 and 2. Additionally, the experimentally observed excitation lifetime of 50–60 ps [79, 84] is also satisfactorily matched here (excitation lifetime of 62.5–76.6 ps was computed as listed in tables 1 and 2). We note that differences between the calculated and experimentally measured rate constants and lifetimes stem from the choice of input parameters in the calculations. Since in the present study we aim to compare theoretical methodologies and BChl organizations, for the purpose of consistency, the set of input parameters from prior publications [9, 19] was adopted here without further adjustment.

### 3.4. Rotation of the RC within the LH1 rings

The question naturally arises whether the theoretical descriptions employed here can discriminate rotation of the RCs within their respective LH1 rings, as depicted in figure 2(d). The rationale for such rotation is that the relative orientation of the RCs within the LH1 rings has been identified in the 2D projection map [23] and through linear dichroism study [29] and, hence, can serve as a test of the present theoretical method. Rotation of the RC within each LH1 ring produces varying LH efficiencies, and one expects that the rotation orientation observed in [23, 29] is optimal, i.e. corresponds to the highest quantum yield [85].

The result of our analysis is portrayed in figure 5. Excitation lifetime was calculated using GF theory over the range of RC rotation angles 0–360°, with 0° corresponding to the RC orientation seen in [23]. The two RCs were rotated to the same degree, but in opposite directions, with the midpoint between the Mg atoms of the special pair BChls used as the locus of the (perpendicular) rotation axes. The calculations were carried out for two organizations of the LH1 BChl array, shown in figures 2(b) and (c). In either case, the excitation lifetime of the core complex changed with the rotation of the RCs by as much as 6 ps, with the shortest lifetime occurring at zero RC rotation, i.e. for the previously reported RC orientation [23, 29] (figure 5(a)). The corresponding changes in the LH efficiency with RC rotation are shown in figure 5(b). One recognizes that the RC orientation reported in [23], indeed, is optimal for the core complex, which confirms our calculations. Similar calculations on RC orientation versus photosynthetic optimality were reported by Geyer in [85], where the same conclusion was reached.
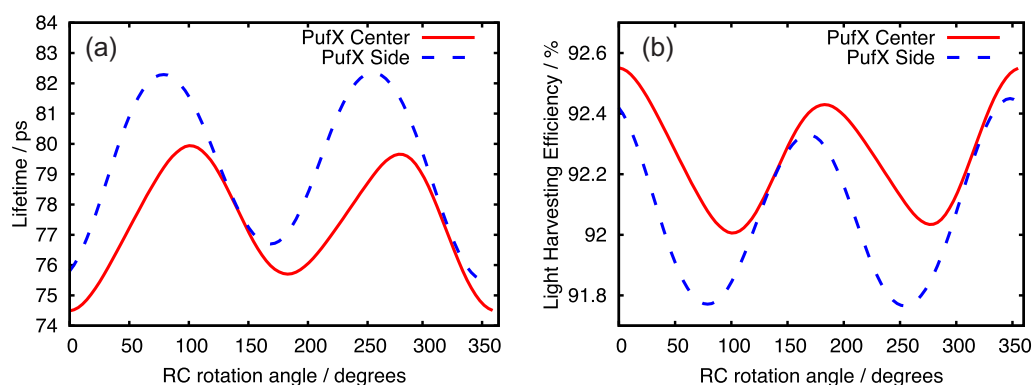
**Figure 5.** Excitation lifetime (a) and LH efficiency (b) as a function of RC rotation angle (figure 2(d)) for both placements of PufX. 'PufX Center' corresponds to the placement of PufX at the center of the core complex [24, 25]; 'PufX Side' corresponds to the placement of PufX near the gaps of LH1 [23].
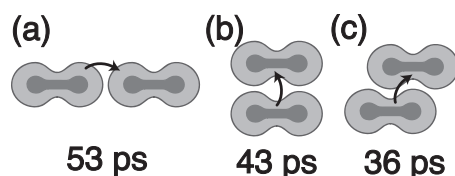


**Figure 6.** Excitation transfer times between neighboring core complexes in different arrangements. (a) Side-by-side placement along the long axis of the core complex results in the longest inter-complex transfer time. (b) Vertically stacked placement produces an intermediate transfer time. (c) Shifted-stacked placement exhibits the shortest transfer time. The nearest inter-complex BChl distance was kept at 27 Å in all placements.

### 3.5. Inter-complex excitation transfer

We calculated the excitation transfer times between neighboring complexes using GF theory for three alternate placements, as depicted in figure 6. In the first placement, core complexes are placed side by side along their dimer axis, in which case the calculated excitation transfer time is 53 ps (figure 6(a)). The respective transfer time in the case of a 'stacking' arrangement of dimers (figure 6(b)), i.e. placing core complexes along their short axis, is 43 ps. When a slight offset is introduced in the stacking arrangement of the core complexes, the excitation transfer time is shortened further to 36 ps (figure 6(c)). In going from placements (a) to (b) in figure 6, the complexes are packed more densely, the average inter-complex BChl distance decreases and, thus, the transfer time shortens. Indeed, in native *Rba. sphaeroides* photosynthetic membranes, the core complex dimers are seen to form tightly packed linear arrays, i.e. as in the case of figure 6(c) [86].

### 3.6. Excitonic properties of the tubular photosynthetic membrane

The core complex-only photosynthetic membrane was constructed according to an EM image of the *Rba. sphaeroides* tubular membrane [17] that displayed a long-range organization of
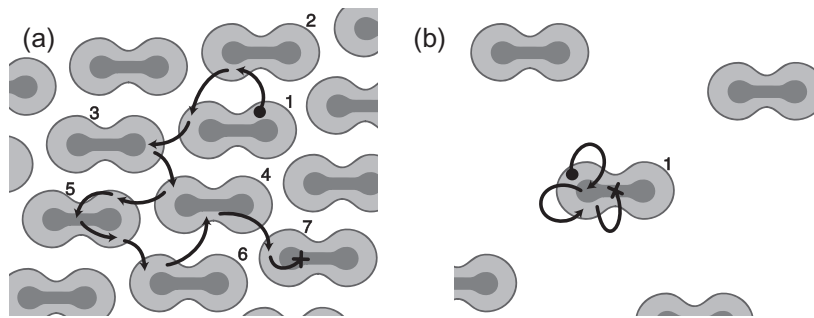
**Figure 7.** A single realization of the random walk on a densely packed tubular photosynthetic membrane (a) and on a sparsely packed tubular photosynthetic membrane (b). Light gray represents the LH1 BChls and darker gray the RC BChls. Initial light absorption is marked by a circle, and the final charge separated state is marked by a cross. In (a), the path of the excitation is $LH1_1 \rightarrow LH1_2 \rightarrow LH1_1 \rightarrow LH1_3 \rightarrow LH1_4 \rightarrow LH1_5 \rightarrow RC_5 \rightarrow LH1_5 \rightarrow LH1_6 \rightarrow LH1_4 \rightarrow LH1_7 \rightarrow RC_7$. In (b), the excitation stays within the same core complex, undergoing the path $LH1_1 \rightarrow RC_1 \rightarrow LH1_1 \rightarrow RC_1$.

helically stacked core complex dimers similar to the ones seen in prior studies [15, 16]. The coordinates of each core complex were taken from [19], as described in section 2, i.e. using the core complex model with 56 LH1 BChls and PufX placed near the gaps of LH1 (figure 2(a)). The resulting model of the photosynthetic membrane is shown in figure 4. Transfer rates determined according to the GF theory were used to calculate the LH efficiency and average excitation lifetime following [9]. For the tubular photosynthetic membrane depicted in figure 4, the average excitation lifetime was found to be 72 ps, indeed comparable to the lifetime of a single core complex as shown in tables 1 and 2. An example path of an excitation is depicted in figure 7(a), showing how an excitation goes through an 11-step random walk across seven different core complexes before reaching a charge-separated state. One of the steps actually involves an RC → LH1 back transfer. The average LH efficiency in this photosynthetic membrane was calculated to be 92.6%.

A second model of the tubular photosynthetic membrane was constructed using the same long-range organization for the core complexes, but with the BChl organization in which PufX interrupts the LH1 BChls at the dimerizing junction of the complex (figure 2(c)). The average excitation lifetime was computed again for this array, resulting in a value of 74 ps, which compares closely with the 72 ps of the first model. It seems that placement of PufX in the core complex has no significant effect either on the energy transfer properties within a single core complex (cf tables 1 and 2) or within the whole core complex-only photosynthetic membrane. As presented in tables 1 and 2, the only discernible difference between side and center placement of PufX is in the transfer rate constants between the halves of the RC and of LH1 ($k_{LH1 \rightarrow LH1}$ and $k_{RC \rightarrow RC}$). The long LH1–RC transfer time and the short RC–LH1 transfer time, both of which do not depend on the PufX placement, dominate the excitation capture process, effectively 'washing out' the difference in $k_{LH1 \rightarrow LH1}$ and $k_{RC \rightarrow RC}$, resulting in the similarity of the overall excitonic property seen in the two different tubular photosynthetic membrane models.

A third model of the photosynthetic membrane was considered. In this model, the BChl array from [19] was used again, but the long-range organization of the complexes was altered

by removing the nearest-neighbor complexes, leaving only the next nearest neighbors, as shown in figure 7(b). In this case, the inter-complex excitation transfer time is longer than 7 ns, even for the closest core complexes, yet the excitation lifetime for this membrane is calculated to be 75.8 ps, with an LH efficiency of 92.3% that is as high as for a densely packed membrane. The efficiencies are identical since there is negligible excitation transfer between different complexes in case of the sparsely packed membrane, and the long (7 ns) inter-complex transfer time does not come into play. As illustrated in figure 7(b), an excitation does not travel to other core complexes, i.e. charge separation occurs within the RCs of the initially excited core complex. This result implies that excitation transfer from LH1 to RC does not rely on closely packed core complexes. The clustering of the core complexes into tightly packed tubular arrays seen in EM imaging of photosynthetic membranes is, therefore, not a result of optimization of the excitation transfer function, but possibly arises to increase the BChl density such that more light is absorbed [9, 17, 87, 88]. Furthermore, a densely packed system of core complexes has the advantage that any core complex with 'busy' or damaged RCs can still contribute its LH1 for LH. Such a core complex has zero quantum yield in a loosely packed situation, but a quantum yield near one in a densely packed situation. Clustering of core complexes is also potentially driven by the intrinsic curvature properties of the core complexes [20, 88].

## 4. Conclusion

In this study, we have constructed an atomic model for the tubular photosynthetic membrane of *Rba. sphaeroides*, composed of solely (RC–LH1–PufX)$_2$ core complexes in an ordered array. The atomic model enables identification of the geometry of the BChl array, consequently used for calculation of the energy transfer kinetics of the full tubular vesicle. Comparison of theoretical approaches indicates that the results from solving the HEOM, computationally very expensive, but accurate, agree closely with the computationally cheap GF theory, thus validating earlier descriptions of energy transfer processes that employed the GF theory (see e.g. [9, 19, 47, 89]; for reviews see [3]–[5], [8]), and justifying further use of the GF approach. The same conclusion was reached previously for excitation dynamics in LH2 and between pairs of LH2 [12].

We note that the environmental fluctuations in different BChls may not be entirely uncorrelated [70], as assumed in this work. The effect of correlated fluctuations is currently under investigation.

There are some uncertainties in the precise molecular arrangement of the *Rba. sphaeroides* core complex, and for this reason our calculations also investigated two different BChl arrangements according to the two RC–LH1–PufX core complex organizations proposed. The results show that the key energy transfer properties of the core complex are largely unaffected by differences in the BChl organization caused by PufX placement and BChl stoichiometry.

With the wealth of structural data on photosynthetic proteins available today, construction of a comprehensive model for the machinery that drives the conversion of energy in living organisms has finally become possible. The necessary large-scale modeling requires structural information for all proteins (and relevant pigments). Although currently we are in an unprecedented fortunate position in terms of available structural information, there are still unknown molecular features that require further resolution. We have demonstrated here, however, that for physiologically relevant cellular properties, a lack of minute detail might not hinder an accurate description. In the present case, we have a clearly defined long-range

**IOP** Institute of Physics ❶ DEUTSCHE PHYSIKALISCHE GESELLSCHAFT

supramolecular organization of the photosynthetic membrane consisting of only the bacterial core complexes. The packing of the tubular membrane is well understood, given available EM images, yet the local molecular details of the complex have not been fully revealed. We show here that the energy transfer properties of the large array of complexes are mostly insensitive to local disturbance of geometry. Such robustness of cellular properties to small-scale alterations, e.g. due to naturally arising radiation damage, is seen in other photosynthetic organisms [89]–[91], and makes a case for pursuing investigations of the functional and structural properties of large molecular assemblies, even when high-resolution data might not yet be available for some of the components.

## Acknowledgments

## References

[1] Blankenship R E 2002 *Molecular Mechanisms of Photosynthesis* (Malden, MA: Blackwell Science)
[2] Schulten K 1999 From simplicity to complexity and back: function, architecture and mechanism of light harvesting systems in photosynthetic bacteria *Simplicity and Complexity in Proteins and Nucleic Acids* ed H Frauenfelder, J Deisenhofer and P G Wolynes (Berlin: Dahlem University Press) pp 227–53
[3] Hu X, Ritz T, Damjanović A, Autenrieth F and Schulten K 2002 *Q. Rev. Biophys.* **35** 1–62
[4] Cogdell R J, Gall A and Köhler J 2006 *Q. Rev. Biophys.* **39** 227–324
[5] Hu X, Damjanović A, Ritz T and Schulten K 1998 *Proc. Natl Acad. Sci. USA* **95** 5935–41
[6] Damjanović A, Ritz T and Schulten K 1999 *Phys. Rev.* E **59** 3293–311
[7] Ritz T, Damjanović A, Schulten K, Zhang J and Koyama Y 2000 *Photosyn. Res.* **66** 125–44
[8] Şener M and Schulten K 2005 Physical principles of efficient excitation transfer in light harvesting *Energy Harvesting Materials* ed D L Andrews (Singapore: World Scientific) pp 1–26
[9] Sener M K, Olsen J D, Hunter C N and Schulten K 2007 *Proc. Natl Acad. Sci. USA* **104** 15723–28
[10] Damjanović A, Ritz T and Schulten K 2000 *Biophys. J.* **79** 1695–705
[11] Scheuring S, Lévy D and Rigaud J-L 2005 *Biochim. Biophys. Acta* **1712** 109–27
[12] Strümpfer J and Schulten K 2009 *J. Chem. Phys.* **131** 225101
[13] Kiley P J, Varga A and Kaplan S 1988 *J. Bacteriol.* **170** 1103–15
[14] Hunter C N, Pennoyer J D, Sturgis J N, Farrelly D and Niederman R A 1988 *Biochemistry* **27** 3459–67
[15] Jungas C, Ranck J, Rigaud J, Joliot P and Verméglio A 1999 *EMBO J.* **18** 534–42
[16] Siebert C A, Qian P, Fotiadis D, Engel A, Hunter C N and Bullough P A 2004 *EMBO J.* **23** 690–700
[17] Qian P, Bullough P A and Hunter C N 2008 *J. Biol. Chem.* **283** 14002–11
[18] Chandler D, Hsin J, Harrison C B, Gumbart J and Schulten K 2008 *Biophys. J.* **95** 2822–36
[19] Sener M K, Hsin J, Trabuco L G, Villa E, Qian P, Hunter C N and Schulten K 2009 *Chem. Phys.* **357** 188–97
[20] Hsin J, Gumbart J, Trabuco L G, Villa E, Qian P, Hunter C N and Schulten K 2009 *Biophys. J.* **97** 321–9
[21] Humphrey W, Dalke A and Schulten K 1996 *J. Mol. Graph.* **14** 33–8
[22] Holden-Dye K, Crouch L I and Jones M R 2008 *Biochim. Biophys. Acta* **1777** 613–30
[23] Qian P, Hunter C N and Bullough P A 2005 *J. Mol. Biol.* **349** 948–60
[24] Scheuring S, Francia F, Busselez J, Melandris B A, Rigaud J-L and Levy D 2004 *J. Biol. Chem.* **279** 3620–6
[25] Scheuring S, Busselez J and Lévy D 2005 *J. Biol. Chem.* **280** 1426–31
[26] Scheuring S 2006 *Curr. Opin. Chem. Biol.* **10** 387–93
[27] Busselez J, Cottevielle M, Cuniasse P, Gubellini F, Boisset N and Lévy D 2007 *Structure* **15** 1674–83
[28] Hsin J, Chipot C and Schulten K 2009 *J. Am. Chem. Soc.* **131** 17096–8

**IOP** Institute of Physics · DEUTSCHE PHYSIKALISCHE GESELLSCHAFT

[29] Frese R, Olsen J, Branvall R, Westerhuis W, Hunter C and van Grondelle R 2000 *Proc. Natl Acad. Sci. USA* **97** 5197–202
[30] Abresch E C, Axelrod H L A, Beatty J T, Johnson J A, Nechushtai R and Paddock M L 2005 *Photosyn. Res.* **86** 61–70
[31] Förster T 1948 *Ann. Phys., Lpz.* **2** 55–75
[32] Redfield A G 1965 *Adv. Magn. Reson.* **1** 1
[33] Yang M and Fleming G R 2002 *Chem. Phys.* **282** 163–80
[34] Ishizaki A and Fleming G R 2009 *J. Chem. Phys.* **130** 234110–8
[35] Tanimura Y and Kubo R 1989 *J. Phys. Soc. Japan* **58** 1199–206
[36] Ishizaki A and Tanimura Y 2005 *J. Phys. Soc. Japan* **74** 3131–4
[37] Ishizaki A and Fleming G R 2009 *J. Chem. Phys.* **130** 234111–10
[38] Conroy M J, Westerhuis W, Parkes-Loach P S, Loach P A, Hunter C N and Williamson M P 2000 *J. Mol. Biol.* **298** 83–94
[39] Tunnicliffe R B, Ratcliffe E C, Hunter C N and Williamson M P 2006 *FEBS Lett.* **580** 6967–71
[40] Ermler U, Fritzsch G, Buchanan S K and Michel H 1994 *Structure* **2** 925–36
[41] Camara-Artigas A, Brune D and Allen J P 2002 *Proc. Natl Acad. Sci. USA* **99** 11055–60
[42] Wang Z Y, Gokan K, Kobayashi M and Nozawa T 2005 *J. Mol. Biol.* **347** 465–77
[43] Trabuco L G, Villa E, Mitra K, Frank J and Schulten K 2008 *Structure* **16** 673–83
[44] Wells D, Abramkina V and Aksimentiev A 2007 *J. Chem. Phys.* **127** 125101–10
[45] Trabuco L G, Villa E, Schreiner E, Harrison C B and Schulten K 2009 *Methods* **49** 174–80
[46] Loach P A 2000 *Proc. Natl Acad. Sci. USA* **97** 5016–18
[47] Hu X, Ritz T, Damjanović A and Schulten K 1997 *J. Phys. Chem.* B **101** 3854–71
[48] Ritz T, Hu X, Damjanović A and Schulten K 1998 *J. Lumin.* **76–77** 310–21
[49] Hu X and Schulten K 1998 *Biophys. J.* **75** 683–94
[50] Sundström V, Pullerits T and van Grondelle R 1999 *J. Phys. Chem.* B **103** 2327–46
[51] Scholes G, Gould I, Cogdell R and Fleming G 1999 *J. Phys. Chem.* B **103** 2543–53
[52] Damjanović A, Ritz T and Schulten K 2000 *Int. J. Quantum Chem.* **77** 139–51
[53] Tretiak S, Middleton C, Chernyak V and Mukamel S 2000 *J. Phys. Chem.* B **104** 9540–53
[54] Ritz T, Park S and Schulten K 2001 *J. Phys. Chem.* B **105** 8259–67
[55] Şener M and Schulten K 2002 *Phys. Rev.* E **65** 031916
[56] Damjanović A, Kosztin I, Kleinekathoefer U and Schulten K 2002 *Phys. Rev.* E **65** 031919
[57] Rutkauskas D, Novoderezhkin V, Cogdell R J and van Grondelle R 2005 *Biophys. J.* **88** 422–35
[58] van Grondelle R and Novoderezhkin V I 2006 *Phys. Chem. Chem. Phys.* **8** 793–807
[59] Sumi H 1999 *J. Phys. Chem.* B **103** 252–60
[60] Scholes G D, Jordanides X J and Fleming G R 2001 *J. Phys. Chem.* B **105** 1640–51
[61] Jang S, Newton M D and Silbey R J 2004 *Phys. Rev. Lett.* **92** 218301
[62] Scholes G D 2003 *Annu. Rev. Phys. Chem.* **54** 57–87
[63] Şener M K and Schulten K 2008 From atomic-level structure to supramolecular organization in the photosynthetic unit of purple bacteria *The Purple Phototrophic Bacteria Advances in Photosynthesis and Respiration* vol 28 ed C N Hunter, F Daldal, M C Thurnauer and J T Beatty (Berlin: Springer) pp 275–94
[64] Kosztin I and Schulten K 2008 Molecular dynamics methods for bioelectronic systems in photosynthesis *Biophysical Techniques in Photosynthesis II, Advances in Photosynthesis and Respiration* vol 26 ed T Aartsma and J Matysik (Dordrecht: Springer) pp 445–64
[65] Weiss U 2008 *Quantum Dissipative Systems* (Singapore: World Scientific)
[66] Zhang W M, Meier T, Chernyak V and Mukamel S 1998 *J. Chem. Phys.* **108** 7763–74
[67] Timpmann K, Trinkunas G, Qian P, Hunter C N and Freiberg A 2005 *Chem. Phys. Lett.* **414** 359–63
[68] Xu R X and Yan Y J 2007 *Phys. Rev.* E **75** 031107–11
[69] May V and Kühn O 2000 *Charge and Energy Transfer Dynamics in Molecular Systems* (Berlin: Wiley)

[70] Freiberg A, Ratsep M, Timpmann K and Trinkunas G 2009 *Chem. Phys.* **357** 102–12

[71] Mohseni M, Rebentrost P, Lloyd S and Aspuru-Guzik A 2008 *J. Chem. Phys.* **129** 174106

[72] Olaya-Castro A, Lee C F, Olsen F F and Johnson N F 2008 *Phys. Rev.* B **78** 085115–7

[73] Schröder M, Schreiber M and Kleinekathöfer U 2007 *J. Chem. Phys.* **126** 114102

[74] Westerhuis W H J, Sturgis J N, Ratcliffe E C, Hunter C N and Niederman R A 2002 *Biochemistry* **41** 8698–707

[75] Grünbaum B and Shephard G C 1987 *Tilings and Patterns* (New York: Freeman)

[76] Keef T, Taormina A and Twarock R 2006 *J. Phys.: Condens. Matter* **18** S375–87

[77] Caspar D L D and Klug A 1962 *Cold Spring Harbor Symp. on Quantitative Biology* vol **27** pp 1–24

[78] Twarock R 2004 *J. Theor. Biol.* **226** 477–82

[79] Sundström V and van Grondelle R 1995 Kinetics of excitation transfer and trapping in purple bacteria *Anoxygenic Photosynthetic Bacteria* ed R Blankenship, M Madigan and C Bauer (Dordrecht: Kluwer) pp 349–72

[80] Visscher K J, Bergstrom H, Sundström V, Hunter C and van Grondelle R 1989 *Photosyn. Res.* **22** 211–7

[81] Freiberg A, Allen J P, Williams J C and Woodbury N W 1996 *Photosyn. Res.* **48** 309–19

[82] Bergström H, van Grondelle R and Sundström V 1989 *FEBS Lett.* **250** 503–8

[83] Sundström V, van Grondelle R, Bergström H, Aakesson E and Gillbro T 1986 *Biochim. Biophys. Acta— Bioener.* **851** 431–46

[84] Beekman L M P, van Mourik F, Jones M R, Visser H M, Hunter C N and van Grondelle R 1994 *Biochemistry* **33** 3143–7

[85] Geyer T 2007 *Biophys. J.* **93** 4374–81

[86] Bahatyrova S, Frese R N, Siebert C A, Olsen J D, van der Werf K O, van Grondelle R, Niederman R A, Bullough P A, Otto C and Hunter C N 2004 *Nature* **430** 1058–62

[87] Geyer T and Helms V 2006 *Biophys. J.* **91** 921–6

[88] Frese R N, Pàmies J C, Olsen J D, Bahatyrova S, van der Weij-de Wit C D, Aartsma T J, Otto C, Hunter C N, Frenkel D and van Grondelle R. 2008 *Biophys. J.* **94** 640–7

[89] Şener M K, Lu D, Ritz T, Park S, Fromme P and Schulten K 2002 *J. Phys. Chem.* B **106** 7948–60

[90] Şener M K, Park S, Lu D, Damjanović A, Ritz T, Fromme P and Schulten K 2004 *J. Chem. Phys.* **120** 11183–95

[91] Yang M, Damjanović A, Vaswani H M and Fleming G R 2003 *Biophys. J.* **85** 140–58